

Green synthesis of CeO₂ nanoparticle like-rose berry using ethanol Extract of *Citrus aurantium* peel and its potential in removal of organic waste

Forat Hamed Kadhem¹; Luma M. Ahmed^{1,2*}; Salam A. Abed³; Afraa Naji Tami²; Wan Mohd Nuzul Hakimi Wan Salleh⁴

1 Department of Chemistry, College of Science, University of Kerbala, Karbala, Iraq.

2 Al-Zahraa Center for Medical and Pharmaceutical Research Sciences (ZCMRS), Al-Zahraa University for Women, Karbala, Iraq.

3 Department of Pharmacognosy, College of Pharmacy, University of Kerbala, Karbala, Iraq.

4 Department of Chemistry, Faculty of Science and Mathematics, University Pendidikan Sultan Idris, Malaysia

*luma.majeed.ahmed@alzahraa.edu.iq

Received: 16 Feb. 2025, Accepted: 28 Mar. 2025. Published: 31 Mar. 2025

ABSTRACT

The take a look at highlights the potential of making use of agricultural by way of-merchandise for sustainable nanoparticle synthesis and their packages in environmental remediation. This paper offers a green synthesis method for (CeO₂) nanoparticles the use of ethanol extract from *Citrus aurantium* peels sourced from Al-Hussainiyah, Iraq. The green synthesis method leverages the herbal antioxidant of *Citrus aurantium* peels, presenting a sustainable and green alternative. The synthesized CeO₂ nanoparticles have been characterized the usage of numerous techniques, along with FTIR spectroscopy, XRD, FE-SEM with (EDX) and BET. The nanoparticles exhibited like-rose berry morphology with a mean crystal size of 12 nm and excessive crystallinity. BET analysis indicated a specific surface area of 173.309m²/g and a mean pore diameter is 3.06nm, ensuring a mesoporous structure. The perfect removal of 10 ppm of eosin yellow dye using 0.025 g of CeO₂ NPs turned into pH 6 at 90 min which agreed with zeta potential analysis, and the adsorption process followed pseudo-second-order kinetics. The ΔH° of adsorption is 13.430 kJ/mol due to this reaction being physical adsorption. The reusability study showed the CeO₂NP could be successfully used up to the 3rd cycle before a loss of 50% from efficiency.

Keywords: Green synthesis, Cerium oxide nanoparticles, Citrus aurantium Peel, Gas Chromatography-Mass Spectrometry, Removal of wastewater.

INTRODUCTION

Green chemistry approach is significant for the future prospect of nanomaterials. This area of nanoscience should culminate in the development of safe, eco-friendly NPs and should have wide acceptance in the nanotechnology [1]. Green synthesis method; provides a faster metallic nanoparticle production by offering an environmentally friendly, simple, economical and reproducible approach. Given the wide range of applications of metallic nanoparticles produced, biological methods play a major role in the synthesis of metallic nanoparticles [2,3] using the extracts from leaves, flowers, roots, peelings, fruits, and seeds of various plants[2]. Green materials contain polyphenols and proteins that can replace chemical reagents as reducing agents to reduce metal ions into lower valence state. In the presence of green materials and under suitable conditions, the quality of green synthesized metal nanoparticles even surpasses those synthesized by chemical methods [4]. Green synthesis has many advantages compared to chemical and physical methods: it is non-toxic, pollution-free, environmentally-friendly, economical, and more sustainable. However, there are issues in the extraction of raw materials, reaction time, and quality of final products. For example, the raw materials are not widely available, the synthesis time is long, and the particle size of the product is highly homogeneous [5]. There have been reports of green syntheses of CeO₂ NPs utilizing microbial, plant, and other biological derivatives. Because of their quantity, safety, and abundance of reducing and stabilizing substances, plants have shown to be the most effective source in this regard [6]. Plant materials including leaves, flowers, and stems have all been utilized to create CeO₂ NPs [7, 8]. Since leaves are a rich source of metabolites, the majority of green synthesis research to far has focused on leaf extracts [7,9]. As reducing and stabilizing agents, a wide range of metabolites/phytochemicals, including ascorbic acid, phenols, ketones, and carboxylic acids, are employed in plant extracts Figure (1).

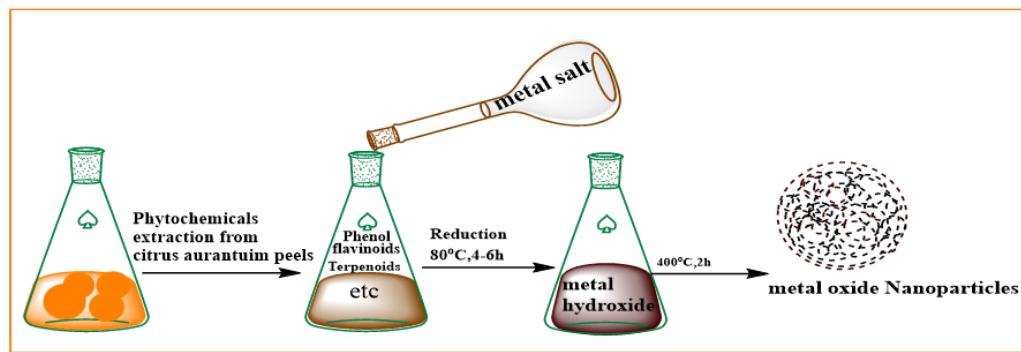


Figure 1: Green synthesis of cerium oxide NPs: Reduction, growth and stabilization

A straightforward method is used to create plant-based CeO₂ NPs: the extract is combined with bulk metal salt, and the reaction takes place in a matter of minutes to several hours under standard laboratory conditions [9-11]. Through the use of phytochemicals, the metallic salt solution is reduced into the corresponding nanoparticles. The production of these nanoparticles is first verified by a change in color from colorless to yellowish, brownish, or whitish, and subsequently described using a variety of spectroscopic and imaging techniques. [7,11, 12]. This study aims to develop a green production method for cerium oxide (CeO₂) nanoparticles utilizing *Citrus aurantuim* peel ethanol extract. This technique aims to provide CeO₂ NPs in an eco-friendly manner by utilizing the inherent antioxidant and reducing properties of *Citrus aurantuim* peels. To optimize the system, the synthesis parameters will be thoroughly examined. The resulting nanoparticles will be characterized by their size, shape, crystallinity, surface properties. The removal of Eosin yellow dye will be examined at optimal conditions.

MATERIAL AND METHODS

The source of *Citrus uranium* peels is Iraq, which served as the renewable uncooked fabric as shown in Figure (2).



Figure 2: *Citrus aurantuim*.

All used reagent and materials were applied without any purification and they illustrated in Table 1.

Table (1) Reagent and materials.

The chemical compounds	Purity	Company
Ethanol	99%	Sigma-Aldrich
Cerium Chloride (III)	99%	Merck, Germany
Eosin yellow dye(C ₂₀ H ₆ Br ₄ Na ₂ O ₅)	99%	BDH, England
Ammonia	35%	BDH, England

Mythology

Extraction of bioactive material from *Citrus aurantuim* peels

The extraction technique was started with the gathering of fresh *Citrus aurantuim* peels. Thorough washing the removal of impurities, and subsequent drying at room temperature for 48 hours were done to eliminate moisture. The 800 g of dried peels was powdered using a mechanical grinder. Consequently, Soxhlet extraction was used to extract the bioactive compounds. Specifically, 370 g of the peel powder underwent extraction with 200 mL of ethanol for 6 hours. Whatman No. 1 filter paper was used to filter the extract in order to remove all solid residue materials, and the extract was then concentrated, yielding an effective source of bioactive compounds.

Green Synthesis of CeO₂ NPs

The steps of the green synthesis of CeO₂ NPs using the ethanol extract for *Citrus aurantuim* peel was displayed in Figure (3).

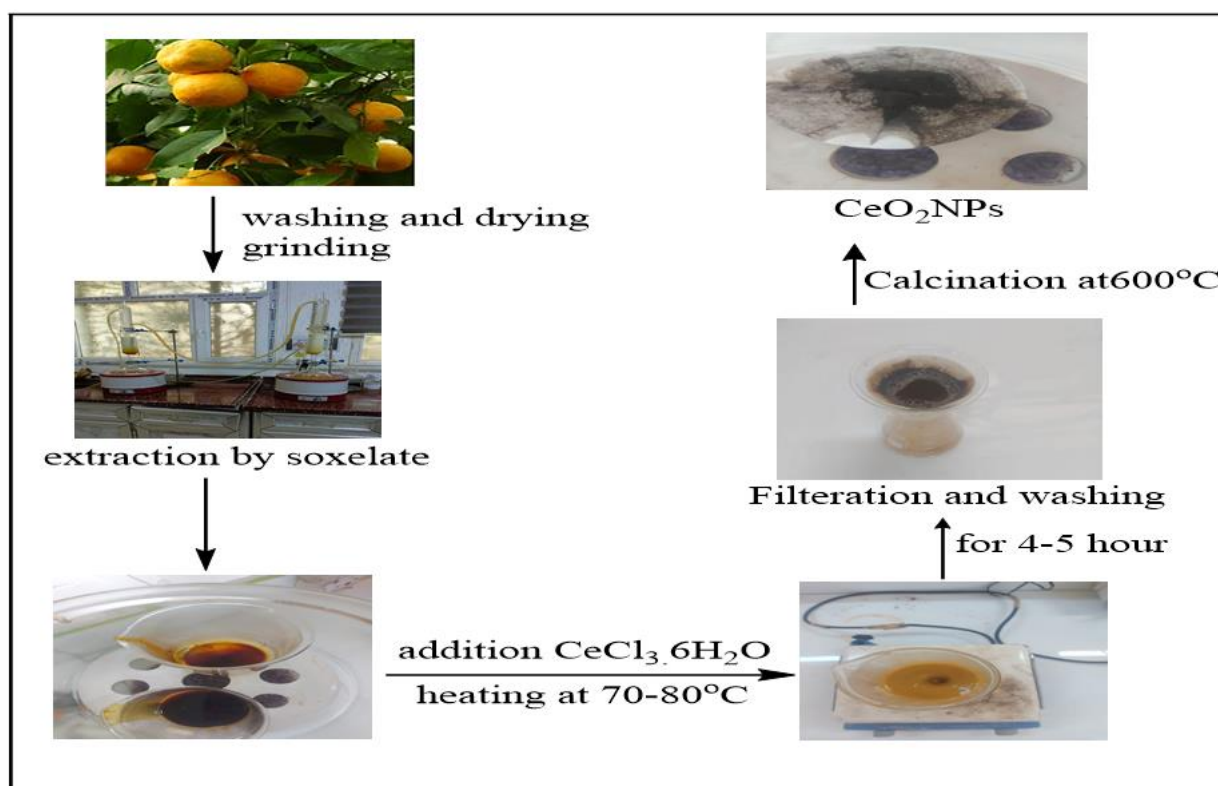


Figure 3: The schematic diagram of green synthesis of CeO₂ NPs using ethanol extract of peels *Citrus aurantuim*.

After collected, washing and drying of *Citrus aurantium* peel, the bioactive compounds were extracted using ethanol. Exact a 1g of the *Citrus aurantium* peel extract was added of cerium ions precursor solution with mixed for 10 min. This step shall allow to interact of the bioactive compounds with cerium ions precursor for beneath non-stop agitation. To facilitate oxide nanoparticle formation, ammonia was steadily adjusted the pH must be between 9 and 10, observed via 20 min of stirring. Heating the aggregate at 80°C for 4-5 hours with continuous stirring triggered, the brown precipitate was occurred. The final precipitate was washed with deionized water to cast off chloride ion residues, followed by way of filtration and drying. Finally, calcination at 600 °C for 3h yielded the desired CeO₂ NPs, prepared for comprehensive characterization.

RESULT AND DISCUSSION

CHARACTRIZATIONS

The bioactive components isolated from *Citrus aurantium* peels were identified and quantified using Gas Chromatography-Mass Spectrometry (GC-MS) analysis. Moreover, series of advanced characterization techniques were employed in order to comprehensively understand the properties and potential applications of the synthesized CeO₂ nanoparticles. These analyses included (FT-IR) spectroscopy, X-ray Diffraction (XRD), field emission Scanning Electron Microscopy (FE-SEM), Energy dispersive x-ray spectroscopy(EDX), Bruner–Emmett–Teller (BET) surface area analysis and Zeta potential analysis. Each technique provided valuable insights into the composition, structure, morphology, and surface characteristics of the nanoparticles, further elucidating their functional capabilities.

GC/MS Analytical of *Citrus aurantium* peel extract using polar solvent (ethanol)

Based on table 2 and figure (4), the bioactive components are essential oils that enhancement the stabilization and detected the shape during growth of CeO₂NPs. The GC/MS Analytical was performed in certain Conditions such as Injection: amount = 1μL Split ratio = 1:5 Heat of injection = 250 °C Column oven: initial temperature is 40 °C increase by 10 °C / min to 60 °C than to 210 °C increase by 5 °C / min to 210 °C Final temperature: increase by 10 °C / min to 280 °C Sample Preparation: 100 μL of the sample is diluted with 5mL of ethanol (HPLC-Grade) before injection. Gas flow ratio: 1 mL/min Pressure: 10 psi m/z Range:1 – 2000. The results demonstrate the presence

of Naringenin in 90.8% , and other alcohols, aldehyde and ketone compounds in good percentages that enhanced the reducing of cerium ions to growth CeO₂ NPs, detecting the shape via growth with a good stabilizing, and prevent the aggregation.

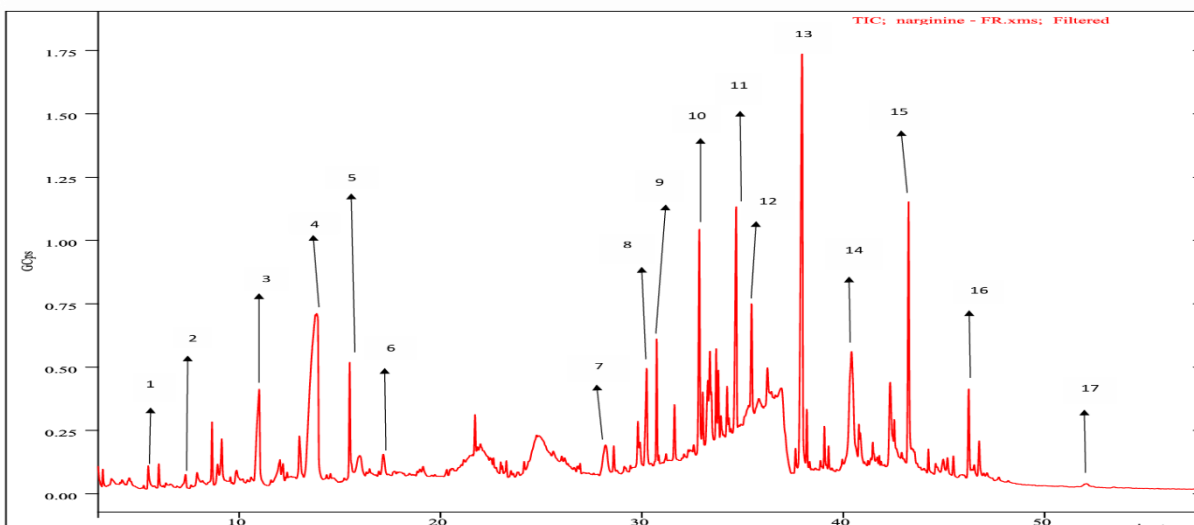


Figure 4: GC/MS Analytical vs time Formulated ethanol extract of peel *Citrus aurantium*.

Table 2: GC/MS Analytical for ethanol extract of peels *Citrus aurantium*

Peak number	Retention time (min)	Area	%Total	M.wt	Prob %	Name
Peak 1	5.491	4.242e+8	0.493	110	84.8	2-Furancarboxaldehyde, 5-methyl
Peak 2	8.654	8.631e+8	1.004	136	21.6	Cyclohexene, 1-methyl-4-(1-methylethenyl)-, (S)-
Peak 3	12.993	1.054e+9	1.226	122	42.0	Benzoic acid
Peak 4	13.789	1.717e+10	19.965	126	83.6	5-Hydroxymethylfurfural
Peak 5	15.492	1.864e+9	2.168	150	55.8	2-Methoxy-4-vinylphenol
Peak 6	21.716	5.563e+8	0.647	122	69.8	Benzaldehyde, 4-hydroxy
Peak 7	28.606	4.130e+8	0.480	162	54.3	7-Hydroxycoumarin
Peak 8	30.240	2.294e+9	2.668	256	87.1	n-Hexadecanoic acid
Peak 9	30.737	1.779e+9	2.069	284	76.4	Hexadecanoic acid, ethyl ester
Peak 10	31.624	9.498e+8	1.105	216	77.9	7H-Furo[3,2-g][1]benzopyran-7-one, 4-methoxy
Peak 11	34.685	4.745e+9	5.519	260	91.0	Isoauraptene
Peak 12	35.450	1.830e+9	2.129	260	87.3	Auraptene
Peak 13	37.957	1.192e+10	13.862	278	97.3	8-(2,3-Dihydroxy-3-methylbutyl)-7-methoxy-2H-chromen-2-one
Peak 14	42.329	2.478e+9	2.882	272	90.8	Naringenin
Peak 15	43.246	4.569e+9	5.315	302	81.3	Hesperetin
Peak 16	46.231	1.481e+9	1.722	414	54.5	γ -Sitosterol
Peak 17	46.750	7.047e+8	0.820	402	97.8	3',4',5,6,7,8-Hexamethoxyflavone

FT-IR spectroscopy

Figure (5) explains the FTIR spectrum of *Citrus aurantiuim* peel extract by ethanol revealed the existence of alcohols and phenols, peaks at 3360cm^{-1} , corresponding to the frequency of O-H bonds and hydroxyl bonds [13]. The C-H stretching vibration is responsible for the peak at 2928 cm^{-1} , indicating the presence of some alkane compounds. The peak at 1639 cm^{-1} could be attributed to the presence of a deformed aromatic ring, amino acids, flavonoids, and stretching vibrations of C=O groups. The identified bands at 1049 cm^{-1} could be due to presence of C–O stretching vibration due to an ester group or secondary alcohol [14].

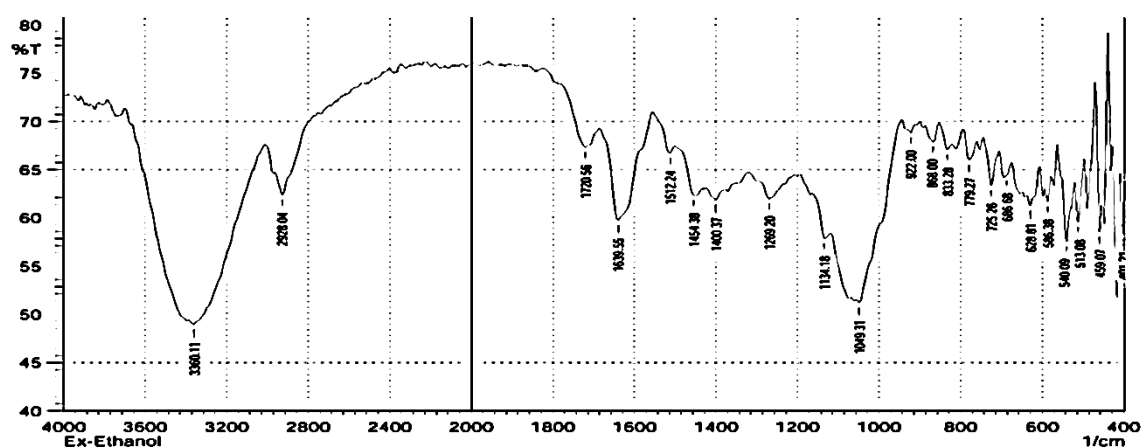


Figure 5: FT-IR spectrum for extracts ethanol of peel *Citrus aurantiuim*.

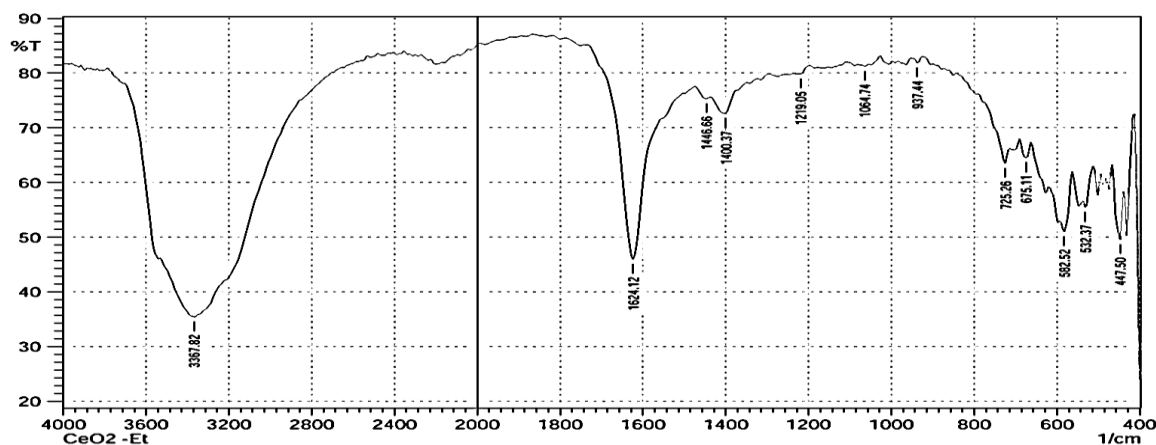


Figure 6: FT-IR spectrum of CeO_2NPs using ethanol extract of peel *Citrus aurantiuim*.

Figure (6) demonstrates the FT-IR spectrum of cerium oxide using ethanol extract. This spectrum indicates to reduce the peaks of active groups of the extractions, the new strong absorption peak at 447.5 cm^{-1} is beyond to Ce-O particles. The peaks at 1400 cm^{-1} and 1219 cm^{-1} indicate to C-H bond oscillation and C-C bond oscillation, respectively [15]. The wide peak at 3367 cm^{-1} and sharp peak at 1624.1 cm^{-1} are similar the position of the oscillation of the O-H bond and H_2O in metal oxide NP[16].

X-ray Diffraction (XRD) Analysis

The XRD analysis of the CeO_2 NPs was explained in Figure (7). The crystal planes of cerium oxide NP observes cubic fluorite at the (111), (200), (220), (311), (222), and (400) are responsible for the 2θ peaks at 28.3° , 36.4° , 49.1° , 58.4° , 65.8° , and 75.2° , respectively (JCPDS-00-034-0394). This results is agreement with results that reported in lecture[16].

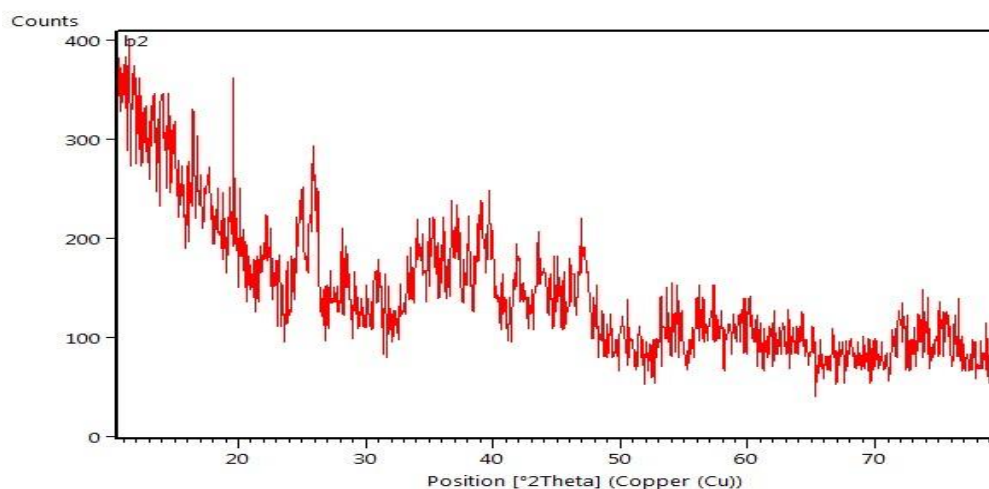


Figure 7: XRD analysis of Green Synthesis CeO_2 NP.

The mean crystal size was calculated using the Scherrer equation [17,18].

$$D = \frac{k\lambda}{\beta \cos\theta} \quad (1)$$

Where D is the crystal size, k is the shape aspect (typically 0.9), λ is the X-ray wavelength (1.5406 \AA for $\text{Cu K}\alpha$), β is the total width at half maximum (FWHM) of the height, and θ is the Bragg attitude.

The XRD data demonstrate the mean crystal size was found to be 12 nm .

FE-SEM of CeO₂ NPs.

Based on Figure (8), the SEM micrograph of the CeO₂ NPs that green synthesis using ethanol extract of peels *Citrus aurantium*, its particles aggregate as rose berry like with particle size range between (30.2-46.3) nm. The particle of CeO₂ NP includes about 3- 4 crystal and that ensure its polycrystalline.

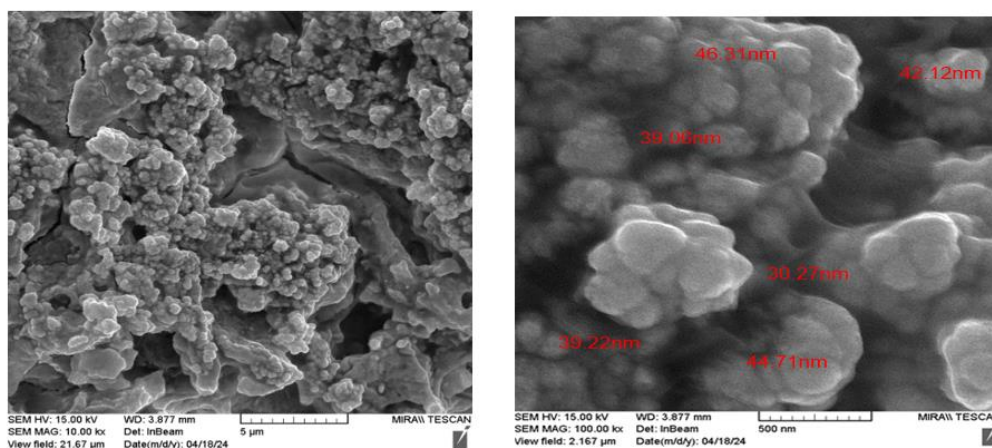


Figure 8: FE-SEM micrographs of Green Synthesis CeO₂ NP.

Energy Dispersive X-ray (EDX) Analysis

The elemental composition of cerium oxide nanoparticles was confirmed by Energy Dispersive X-ray Spectroscopy) in Figure (9). The Ce and O atoms are the main elements in CeO₂ NP sample, but the small amount of C atoms occur via used as substrate in this analysis.

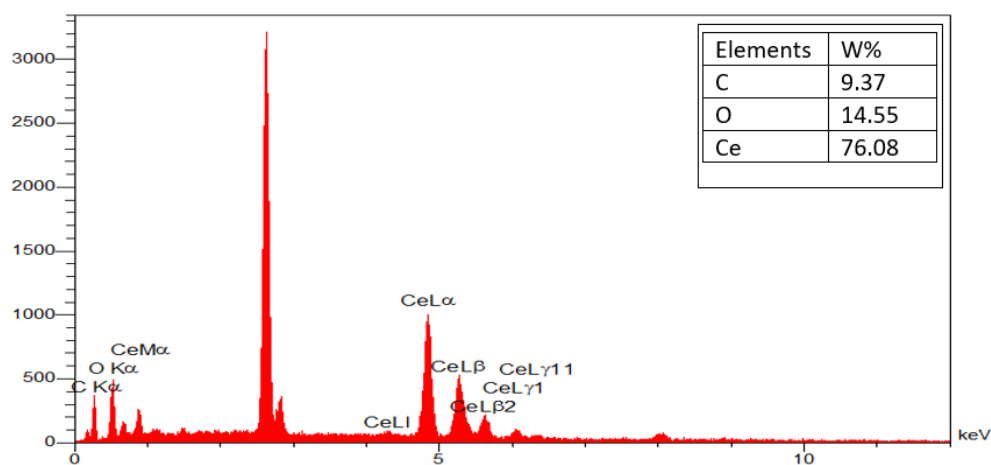


Figure 9: EDX spectrum of Green Synthesis CeO₂ NPs.

N₂ Adsorption - desorption Analysis

N₂ adsorption–desorption analysis can be used to illustrate the specific surface area and the pore size distribution. Specific surface area, average pore volume, and average pore diameter based on the BET plot that based on the data as shown in Figure (10) their pore width distribution remained narrow [19,20].

However, according to the IUPAC classification, the hysteresis loop was within the range of $0.4 < P/P_0 < 1$ and this value was linked to capillary condensation [20, 21]. The sample displayed a type IV isotherm with an H3 hysteresis loop. Based on Figure (10) b, the mesoporous materials have a pore size distribution with a range from 5 to 10 nm [20]. The BET analysis revealed a specific surface area of 173.309m²/g, indicating a reasonable surface area value that is advantageous for catalytic applications. The total pore volume is found to be 0.064 cm³/g and an average pore diameter is equal to 3.06 nm, these results suggest that the nanoparticles have a mesoporous structure [21].

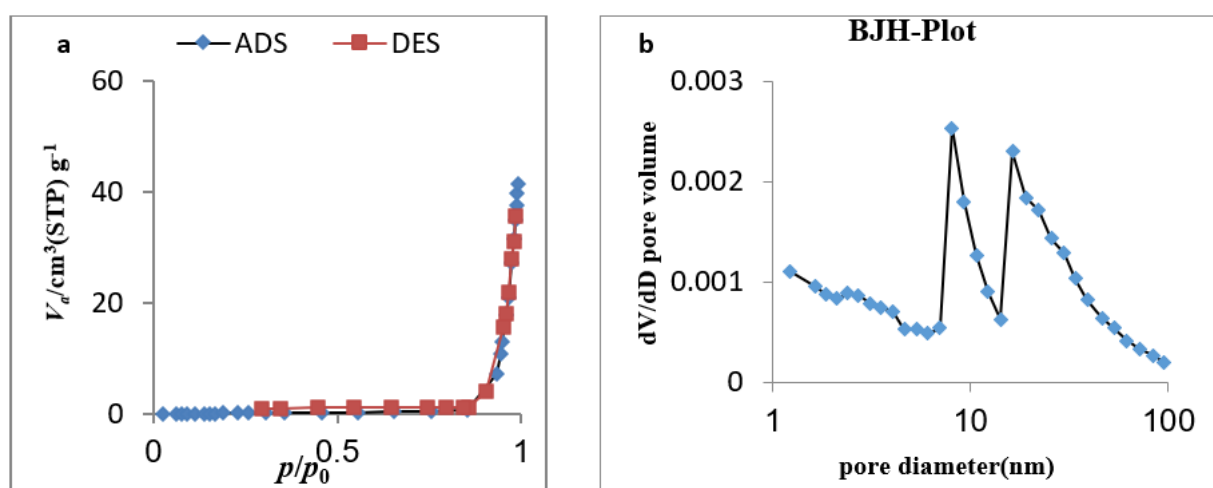


Figure 10: a. N₂ adsorption- desorption isotherms of Green Synthesis CeO₂ nanoparticles. b. the corresponding Barrett-Joyner-Halenda pore size distribution curve of Green Synthesis CeO₂ nanoparticles.

Zeta Potential Analysis

Zeta potential analysis provides significant insights into the surface charge and colloidal stability of synthesized CeO₂ nanoparticles. The zeta potential is an important parameter affecting the diffusion and aggregation behavior of nanoparticles in solution [22]. The results of the zeta potential analysis are presented in Table 3.

Table 3. Zeta Potential Analysis of Green Synthesis CeO₂ nanoparticles.

Sample	pH	Zeta Potential (mV)	Stability
CeO ₂ -NP	3	+15.2	Moderate
	6	+32.8	High
	8	-21.4	Good

At pH 3, CeO₂ NPs exhibited a zeta potential of +15.2 mV, indicating a moderate colloidal state. This positive charge indicates the presence of protonated surface groups, contributing to the electrostatic repulsion between the particles. At pH 6, the zeta potential increased sharply to +32.8 mV, indicating high stability. This pH value is optimal for dispersion and prevention of aggregation of nanoparticles, which is useful for applications that require stable suspensions. At pH 8 the zeta potential is decreased and shifted to -21.4 mV, indicating good stability that due to negative surface charge. The negative charge is apparently, which attitude to the deprotonation from the surface that contains on hydroxyl groups, and then that will lead to generate forces that prevent aggregation[22].

Adsorption activity evaluation

The Adsorption activity study was performed using by filling various volumetric flasks with 25 mL of each of the adsorption solutions of Eosin yellow dye at concentrations ranging from 5, 10, 15, and 20 ppm. These flasks were placed in a water bath with a vibrator at a varied temperature between 283-298 K after these solutions were in contact with (0.010, 0.015, 0.020, and 0.025) g of adsorbent surface (CeO₂ NPs). The pH (3,4,5,6,7, and 8) was used to regulate the acid function for the elimination procedure. The amount of adsorption was then determined when the flasks were removed at contact durations ranging from 15 to 120 minutes. Following the adsorption process, the amount of Eosin yellow dye residue in solution was determined at the maximum wavelength (λ_{\max}), which is 516 nm. Thermodynamic investigations were conducted in stages to determine optimal conditions and temperatures. The adsorption (Removal) efficiency E % can be calculated by following the equation [23, 24]:

$$\text{Removal efficiency (E \%)} = \frac{C_o - C_e}{C_o} \times 100 \quad (2)$$

Where: C_0 , C_e Indicate to the starting concentration and equilibrium concentration of residual dye mg/L.

Contact Time Effect

Figure (11) shows the relationship between contact time and the removal efficiency of 10 mg/L eosin yellow dye using 0.025 g from CeO_2 NPs at 298 K, pH=8 and contact times ranged from 15 to 120 minutes. The removal efficiency elevates with rising contact time from 15 min until reach to 90 min. After 90 min removal efficiency 76.18 % depresses that attitude to rise the kinetic energy for dye molecule to disperse on vacant sites of CeO_2 NP until wholly covered, then agglomerated the dye molecules on surface layer, which leading to elevate the surface energy that caused of returning dye for solution[25, 26].

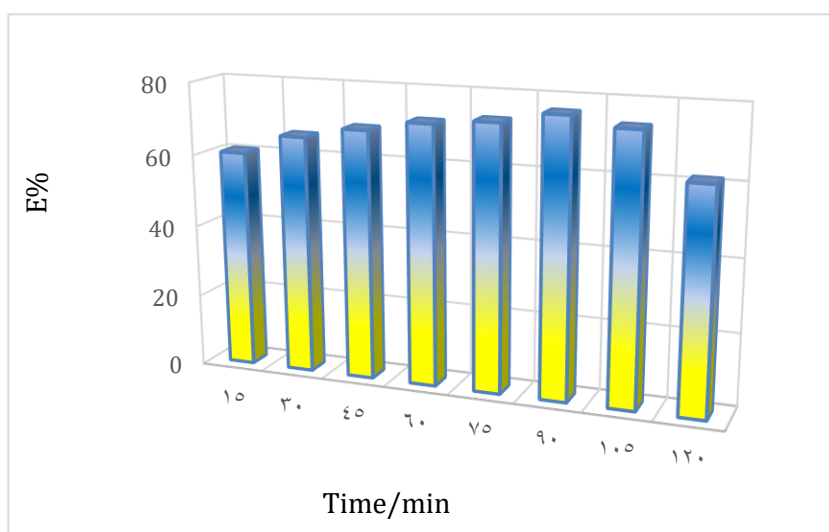


Figure 11: Impact contact time on adsorption process.

Effect Dose of the Adsorbent

Experiments were conducted with CeO_2 nanoparticles weights 0.005, 0.01, 0.015 and 0.025 g, with an initial dye concentration of 10 mg/L at 298K, as shown Figure(12). The data collected showed that the removal rate efficiency increases until reach to 26.18 % at 0.025 g and pH = 8. The results indicated that the rising in CeO_2 NPs dosage led to high adsorption efficiencies because of rising in the ratio of total active surface area with increasing the amount of CeO_2 nanoparticles[27]. Hence, 0.025 g of CeO_2 nanoparticles was chosen as an optimal dose.

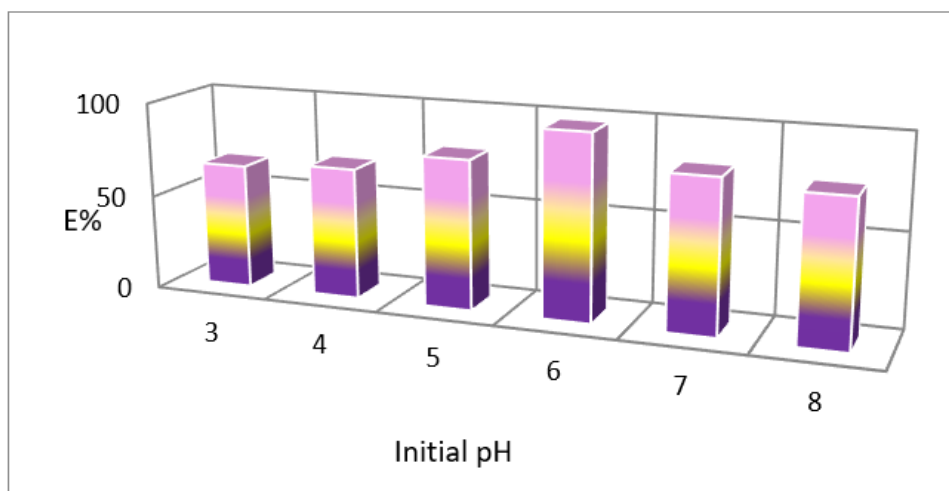


Figure 12: Impact CeO_2 NPs dose on adsorption process.

Effect of initial pH of Eosin yellow dye solution

This parameter shall describe via many phenomena that can be happened, which caused the change in surface charge properties of the nanoparticles and the solubility or ionization state of dye. Figure (13) encapsulates the pivotal role of pH in modulating the adsorption of Eosin yellow dye. The removal efficiency is rapidly increased from pH 3 to pH 6 and gives a maximum adsorption efficiency at 97.48%. The results indicated the maximum adsorption efficiency at pH 6 was accepted with the maximum value result of zeta potential analysis that observed at pH 6. The protonation of surface enhances the anionic dye adsorption owing to the electrostatic attraction [28]. Conversely, the adsorption efficiency diminished from pH 7 to 8 that attitude to excess the hydroxyl ions in surface that increases the repulsive force with this negative dye [29].

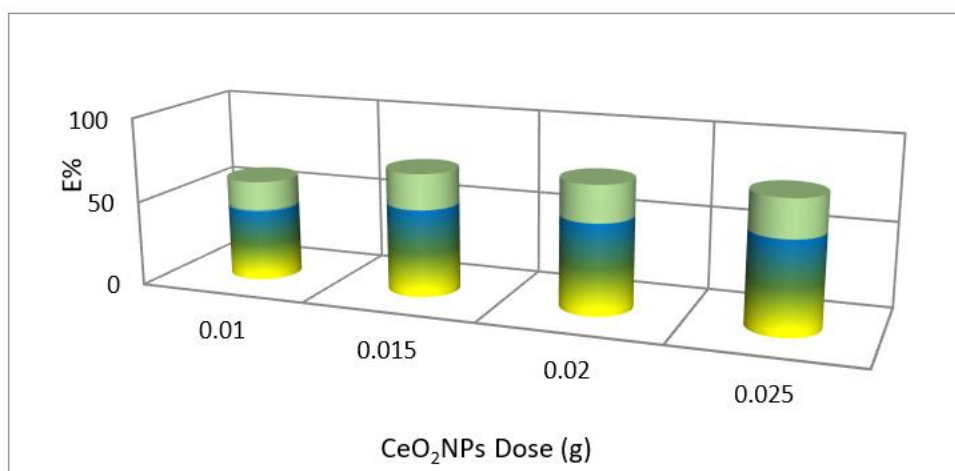


Figure 13: Effect of initial pH of Eosin yellow dye on adsorption process using green synthesis CeO_2

Effect the Temperature

The impact of temperature changes has been studied in order to illustrate and comprehend the nature of the adsorption process. Figure (14) illustrates how temperature affects performance. Gibbs free (ΔG°), enthalpy (ΔH°), and entropy (ΔS°) are examples of thermodynamic parameters that may be determined using equations 3-6 as well as Table (4). The sorption distribution coefficient (k_d) [30,31] was determined.

$$k_d = \frac{Q_e M}{C_e V} \quad (3)$$

Where k_d is the equilibrium constant for the adsorption operation at any temperature, Q_e (mg/g) is the amount of dye adsorbed at equilibrium (adsorbent capacity), C_e (mg/L) the concentration of eosin yellow dye at equilibrium, V is the volume of the solution (L) and M is the mass adsorbed (g).

The Van't Hoff formula was used to estimate the changes in the standard entropy ΔS° and the standard enthalpy ΔH° [32], as shown in Figure (14) A.

$$\ln k_d = \frac{-\Delta H^\circ}{RT} + \frac{\Delta S^\circ}{R} \quad (4)$$

Here, R stands for the universal gas constant (J/mol. K) and T is the absolute temperature in Kelvin.

Using the Nernst equation (equation 5), the standard Gibbs free energy (ΔG°) was determined [32], and the relation between ΔG° and temperature is plotted in Figure (14) B.

$$\Delta^\circ G = -RT \ln K_d \quad (5)$$

Where $\Delta^\circ G$: is a Gibbs energy (kJ/mol), R : is the ideal gas general constant (8.314 J/mol. K), T : is absolute temperature.

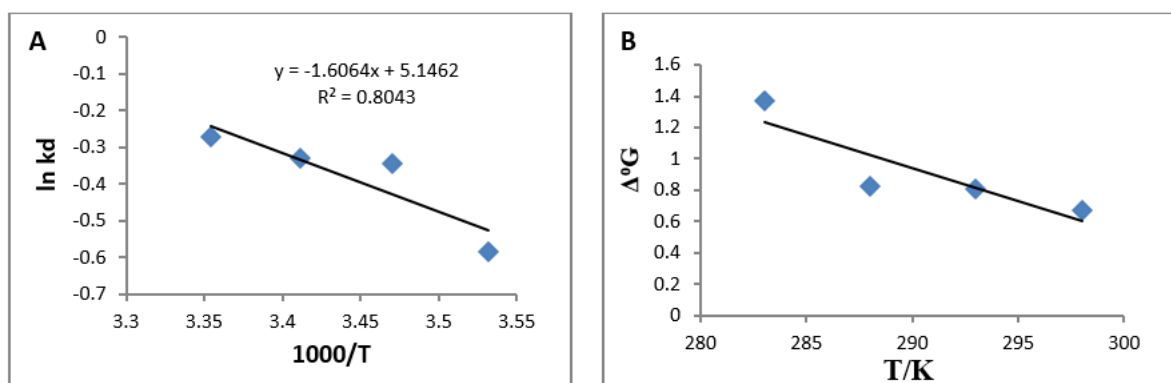


Figure 14: A: Relation between $\ln k_d$ and $(1000/T)$ for adsorption of Eosin yellow dye on CeO_2NPs surface. (B): Relation of ΔG° versus temperature for an endothermic process of adsorption of Eosin yellow dye on CeO_2NPs surface using ethanol extract peel *Citrus aurantium*.

The equation(6)was used to get the activation energy [33].

$$E_a = \Delta H^{\circ} + RT \quad (6)$$

Table 4. Function values ΔG , ΔH and ΔS in Eosin yellow using greenCeO₂NPs of extract ethanol of peel *Citrus aurantuim* (283-298K).

T °C	T K	1000/T (K ⁻¹)	kd	1000/T (K ⁻¹)	ln(kd)	ΔS° kJ/mol.K	ΔG° kJ/mol	Ea kJ/mol	ΔH° kJ/mol
10	283	3.534	0.558	3.533	-0.582	0.0427	1.371	15.708	13.355
15	288	3.472	0.708	3.472	-0.345		0.826	15.750	
20	293	3.413	0.717	3.412	-0.331		0.808	15.791	
25	298	3.356	0.761	3.355	-0.272		0.673	15.833	

Based on Figure14 and Table 4 elucidates the thermodynamic parameters predominated on the adsorption manner. The Gibbs free energy (ΔG°) values are positive indicating the adsorption of Eosin yellow dye by green synthesized CeO₂ NP is a non-spontaneous reaction. The positive ΔH° of this reaction was found to be 13.430 kJ/mol, this value suggests that the adsorption type is physical (less 20 kJ/mol) and the system is endothermic [34,35]. Furthermore, the small value of ΔS° (0.0423 kJ/mol. K) ensures the decline in the randomness of the solid-solution interface in the course of the adsorption system [36]. The values of activation energy ensure the uptake of dye from solution to CeO₂ NP surface is successfully happened.

Isotherm of Adsorption

In this study, Freundlich, Langmuir, and Temkin's isotherm equations were applied to match the experimental data for uptake the eosin dye at different concentrations. The adsorption isotherm describes the relationship between the amount of removed dye and the remaining concentration at equilibrium. This work used non-linear Langmuir and Freundlich models to analyze adsorption isotherm data and characterize the process. The monolayer adsorption of the adsorbate on homogeneous sites within the adsorbent is characterized as:

1. Isotherm Langmuir

The Equation 7 is Langmuir equation, and it represents the adsorption process takes place across homogeneous sites of the adsorbent [37,38].

$$Q_e = \frac{abC_e}{1 + bC_e} \quad (7)$$

Where; Q_e = defined as the quantity of eosin yellow adsorption at the time of equilibrium(mg/g). (a, b) are the constants of Langmuir.

$$R_L = \frac{1}{1 + bC_e} \quad (8)$$

Where: R_L = meaning refer to adsorption kinds is Irreversible ($R_L=0$), Likely ($0 < R_L < 1$) linear ($R_L=1$) [38]. The (a) and (b) values are calculated from the slopes ($1/a$) and intercepts ($1/ab$) of linear plots of C_e/Q_e versus C_e are shown in Figure (15).

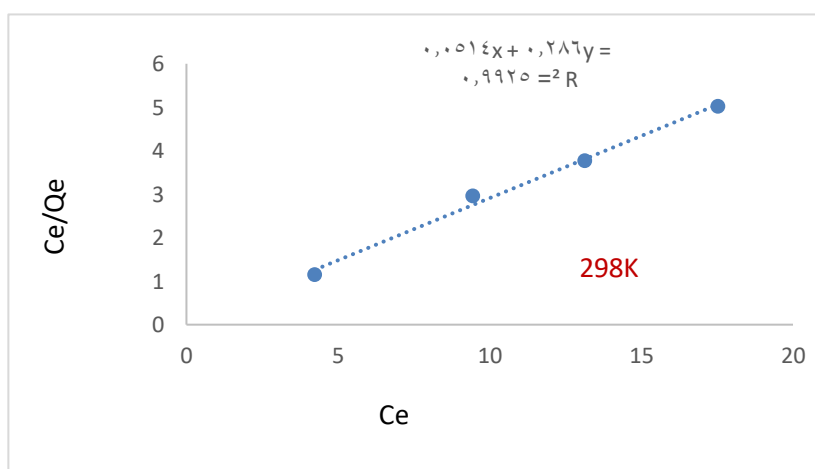


Figure 15: Langmuir isotherms for Eosin yellow dye using the surface of the CeO₂ NPs at 25°C.

1. Isotherm Freundlich

Multi-layered adsorption over heterogeneous active sites is indicated by the Freundlich isotherm pattern of adsorption. Freundlich isothermal. [39].

$$\text{Log}Q_e = \text{Log}K_F + \frac{1}{n}\text{Log}C_e \quad (9)$$

Where: K_F , n = Freundlich's constants. Figure (16) shows the applicability of the Freundlich equation well when plotting $\text{Log} Q_e$ against the values of $\text{Log} C_e$

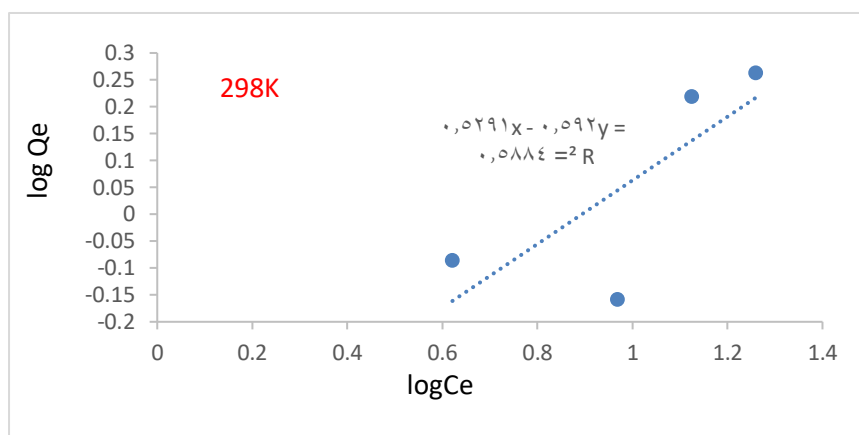


Figure 16: Freundlich isotherm Eosin yellow dye using surface the CeO₂ NPs at 25°C.

1. Temkin Isotherm

The following is how it is frequently used [40]:

$$Q_e = \beta \ln A_T + \beta \ln C_e \quad (10)$$

Where: A_T is the equilibrium binding constant. β = associated with the heat of adsorption. where the eosin yellow dye adsorption Temkin isotherm curves are shown in Figure (17) .

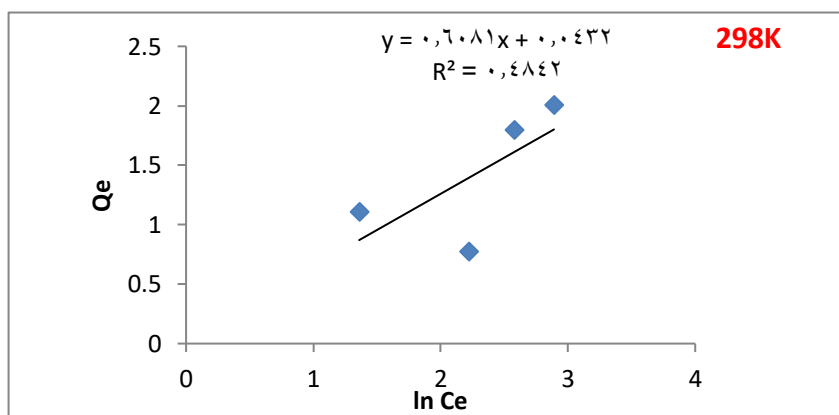


Figure 17: Temkin isotherm eosin yellow dye using the surface of the CeO₂ NPs at 25°C

The (a, b, RL) for Langmuir constants, (n, KF) for the Freundlich pattern and the Temkin pattern constants (β , A_T) with linear correlation coefficients are shown in Table 5.

Table 5. Adsorption isotherm values each of Langmuir, Freundlich, and Temkin at 25°C.

Models	Langmuir isotherm	Models	Freundlich isotherm	Models	Temkin isotherm
a (L/mg)	6.485508	KF	1.890002	β	0.7978
b (mg/g)	3.1328	n	1.689189	A_T	1.34777
R²	0.9994	R²	0.5884	R²	0.4842
R_L	0.015184				

From the results the (R^2) values in Table 5, the Langmuir model is found to be more turned for this adsorption reaction compared with that value of the Freundlich and Temkin models [41]. The Freundlich constant n is found to equal 1.689 that agreement with the actual this reaction is a multilayer (physical adsorption), and this process is favorable for the studied dye because the n value ranges between 1 and 10 [40]. The R_L value is obtained less than 1, hence this reaction is likely [42]. The low values of R^2 indicate to the adsorption of dye on the surface of CeO_2 NPs is heterogeneous.

Effect of Addition the Oxidation Agents on Eosin yellow dye removal process

Figure (18) encapsulates have an impact on supplementary oxidizing dealers, specifically hydrogen peroxide (H_2O_2) and ferrous ions (Fe^{2+}), at the adsorption of eosin yellow dye. The records show that the addition of these oxidizing agents enhanced the adsorption performance, with the Fenton response (related to both H_2O_2 and Fe^{2+}) yielding an outstanding efficiency of 96.37%. This synergistic effect may be ascribed to the era of especially reactive hydroxyl radicals ($\bullet\text{OH}$) through the Fenton technique, which augments the oxidative adsorption of the dye molecules. Consequently, the judicious incorporation of such oxidizing agents presents a viable strategy to further optimize the adsorption performance of the CeO_2 nanoparticles. The results indicate that the addition of hydrogen peroxide alone and ferrous ions alone depress the adsorption efficiency. This behavior due to the Fe^{2+} may be compared to the dye on occupies active sites in the cerium oxide nanoparticles via the adsorption process. Moreover, the H_2O_2 shall oxide the semiconductor surface to give a positive charge with hydroxyl ion and hydroxyl radical, and the last species will adsorption on the surface and decrease the negative dye adsorption (eosin yellow dye) this result is in agreement with result that reported in reference [43]. Whereas, using the Fenton reaction, which involves both H_2O_2 and Fe^{2+} resulted in an adsorption efficiency of 96.37%, very close to the efficiency observed without any

additional oxidizing agents to generate equivalent positive and negative charges at the same time. As in the following equations [44].

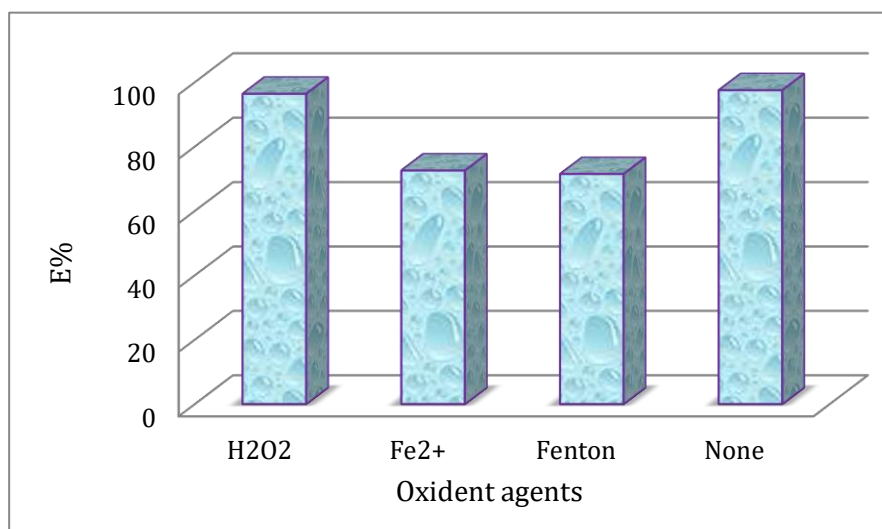
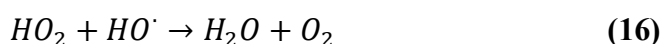
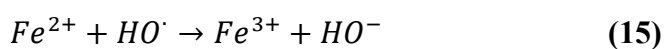
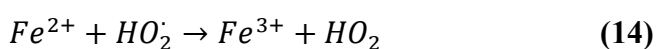
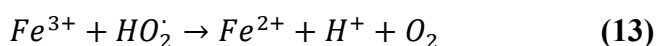
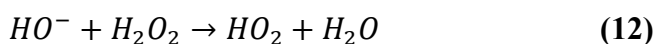
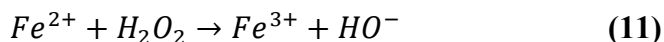


Figure 18: Effect of oxidizing agents on adsorption efficiency of Eosin yellow dye on green synthesis CeO₂ NPs surface at initial pH equal to 6.

Reusability of CeO₂ nanoparticles

The statistics provided in Figure (19) shed mild on the reusability of the synthesized CeO₂ NPs for packages. While the nanoparticles exhibited an impressive 97.48 % removal efficiency performance in the preliminary cycle, a gradual decline in performance was found with subsequent reuse cycles.

This phenomenon can be ascribed to the capacity deactivation by saturated or blocking the active sites of surface by dye molecules, or fouling of the nanoparticle surface, which may restrict the adsorption and adsorption strategies [45]. Nevertheless, the nanoparticle's proven ability to perform well during the first three rounds pastime more than one cycle underscores their potential for sustainable and fee-effective applications. The results indicate a decline in adsorption efficiency with a continuous reuse cycle when used five times. it maintained its warranty until the third time because the dye molecules are gradually accumulating and preventing interaction with the surface [45,46]. However, the nanoparticles still exhibited significant adsorption activity after multiple cycles. The results observed good reusability, which is the acceptable loss in the sorption ability after five circulations.

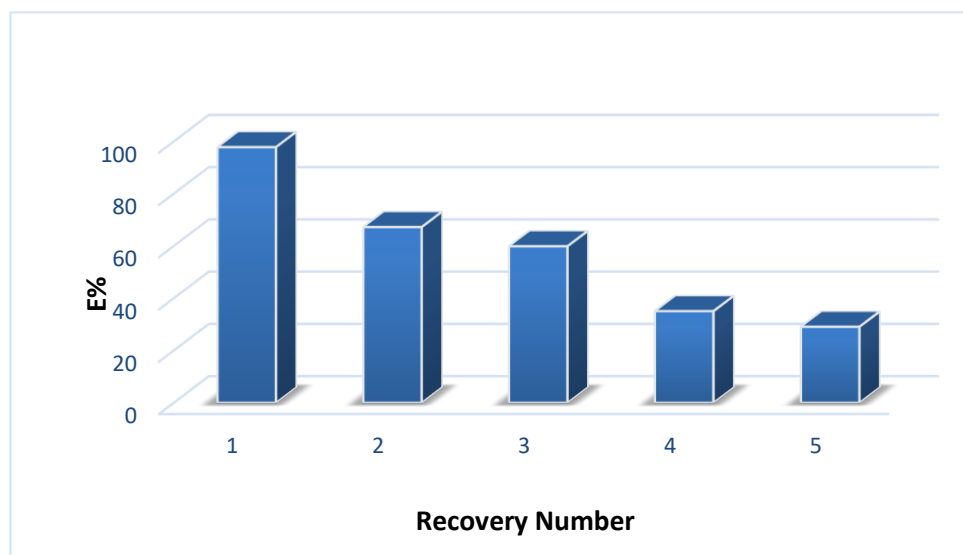


Figure 19: Reusability of CeO₂ NPs surface for Eosin yellow dye adsorption at initial pH equal to 6.

Conclusion

Green synthesis of CeO₂ NPs using *Citrus aurantium* peel extract was successfully prepared and it provided a sustainable and environmentally friendly method. The synthesized CeO₂ NP was characterized by X-ray diffraction (XRD), field emission scanning electron microscopy (FE-SEM), Energy dispersive X-ray spectroscopy (EDX), Bruner–Emmett–Teller (BET) surface area analysis and Zeta potential analysis. Based on the XRD data, the CeO₂ NP structure was estimated as a cubic fluorite with a crystal size of 12 nm. The SEM analysis was proved the shape of CeO₂ NP is like rose

beery. N₂ adsorption – desorption analysis demonstrates the CeO₂ NP is mesoporous, hence, it's can be applied as catalyst to removal a pollutants. The nanoparticles demonstrated good adsorption and antioxidant properties, making them suitable for a wide range of applications and emphasizing the need for further research to fully exploit their advantages. The isothermal fitting was investigated as an appropriate model to express the physical adsorption behavior of dye on synthesized CeO₂ NP this result is agreed with Freundlich result. The thermodynamic study indicated that the adsorption mechanism between synthesized CeO₂ NP and Eosin yellow dye was non- spontaneous and endothermic process. The Adsorption activity was studied by way of the preliminary dye concentration, pH, and temperature. Higher adsorption efficiencies were located at 10 ppm dye concentrations, with a finest pH of 6, and multiplied interest at 25°C temperature. Additionally, the green synthesis technique by leveraging agricultural –products, this observation aims to contribute to sustainable improvement and pollutant reduction, at the same time as exploring the practical packages of green–synthesized CeO₂ NPs in various fields such as environmental remediation.

Acknowledgments: The authors would like to thank all supported people at the University of Karbala and Al-Zahraa Center for Medical and Pharmaceutical Research Sciences (ZCMRS), Al-Zahraa University for Women.

Conflict of Interest: The authors declare no conflict of interest.

References

- [1] Varma, R.S., 2012. Greener approach to nanomaterials and their sustainable applications. *Current Opinion in Chemical Engineering*, 1(2), pp.123-128. <https://doi.org/10.1016/j.coche.2011.12.002>
- [2] Gour, A. and Jain, N.K., 2019. Advances in green synthesis of nanoparticles. *Artificial cells, nanomedicine, and biotechnology*, 47(1), pp.844-851. <https://doi.org/10.1080/21691401.2019.1577878>
- [3] Abed AQ, Hindawi AM, Alesary HF. Synthesis and characterization of zinc sulfide nanomaterials for removal methylene blue dye from aqueous solution. In *AIP Conference Proceedings* 2023 Jul 17 (Vol. 2830, No. 1). AIP Publishing. <https://doi.org/10.1063/5.0156826>

- [4] Ying, S., Guan, Z., Ofoegbu, P.C., Clubb, P., Rico, C., He, F. and Hong, J., 2022. Green synthesis of nanoparticles: Current developments and limitations. *Environmental Technology & Innovation*, 26, p.102336. <https://doi.org/10.1016/j.eti.2022.102336>
- [5] Perveen, R., Shujaat, S., Qureshi, Z., Nawaz, S., Khan, M.I. and Iqbal, M., 2020. Green versus sol-gel synthesis of ZnO nanoparticles and antimicrobial activity evaluation against panel of pathogens. *Journal of Materials Research and Technology*, 9(4), pp.7817-7827. <https://doi.org/10.1016/j.jmrt.2020.05.004>
- [6] Singh, A., Hussain, I., Singh, N.B. and Singh, H., 2019. Uptake, translocation and impact of green synthesized nanoceria on growth and antioxidant enzymes activity of *Solanum lycopersicum* L. *Ecotoxicology and environmental safety*, 182, p.109410. <https://doi.org/10.1016/j.ecoenv.2019.109410>
- [7] Maqbool, Q., Nazar, M., Naz, S., Hussain, T., Jabeen, N., Kausar, R., Anwaar, S., Abbas, F. and Jan, T., 2016. Antimicrobial potential of green synthesized CeO₂ nanoparticles from *Olea europaea* leaf extract. *International journal of nanomedicine*, pp.5015-5025. <https://www.tandfonline.com/doi/epdf/10.1076/0271-3683%28200004%292041-5FT276?needAccess=true>
- [8] Nadaroglu, H., Onem, H. and Alayli Gungor, A., 2017. Green synthesis of Ce₂O₃ NPs and determination of its antioxidant activity. *IET nanobiotechnology*, 11(4), pp.411-419. <https://doi.org/10.1049/iet-nbt.2016.0138>
- [9] Sisubalan, N., Ramkumar, V.S., Pugazhendhi, A., Karthikeyan, C., Indira, K., Gopinath, K., Hameed, A.S.H. and Basha, M.H.G., 2018. ROS-mediated cytotoxic activity of ZnO and CeO₂ nanoparticles synthesized using the *Rubia cordifolia* L. leaf extract on MG-63 human osteosarcoma cell lines. *Environmental Science and Pollution Research*, 25, pp.10482-10492. <https://doi.org/10.1007/s11356-017-0003-5>
- [10] Malleshappa, J., Nagabhushana, H., Prashantha, S.C., Sharma, S.C., Dhananjaya, N., Shivakumara, C. and Nagabhushana, B.M., 2014. Eco-friendly green synthesis, structural and photoluminescent studies of CeO₂: Eu³⁺ nanophosphors using *E. tirucalli* plant latex. *Journal of alloys and compounds*, 612, pp.425-434. <https://doi.org/10.1016/j.jallcom.2014.05.101>

- [11] Singh, A., Hussain, I., Singh, N.B. and Singh, H., 2019. Uptake, translocation and impact of green synthesized nanoceria on growth and antioxidant enzymes activity of *Solanum lycopersicum* L. *Ecotoxicology and environmental safety*, 182, p.109410. <https://doi.org/10.1016/j.ecoenv.2019.109410>
- [12] Rajan, A.R., Rajan, A., John, A. and Philip, D., 2019, May. Green synthesis of CeO_2 nanostructures by using *Morus nigra* fruit extract and its antidiabetic activity. In AIP conference proceedings (Vol. 2105, No. 1). AIP Publishing. <https://doi.org/10.1063/1.5100693>
- [13] Aseyd Nezhad, S., Es-haghi, A. and Tabrizi, M.H., 2020. Green synthesis of cerium oxide nanoparticle using *Origanum majorana* L. leaf extract, its characterization and biological activities. *Applied Organometallic Chemistry*, 34(2), p.e5314. <https://doi.org/10.1002/aoc.5314>
- [14] Widadalla, H.A., Yassin, L.F., Alrasheid, A.A., Ahmed, S.A.R., Widadallah, M.O., Eltilib, S.H. and Mohamed, A.A., 2022. Green synthesis of silver nanoparticles using green tea leaf extract, characterization and evaluation of antimicrobial activity. *Nanoscale Advances*, 4(3), pp.911-915. <https://doi.org/10.1039/D1NA00509J>
- [15] Khan, H., Yerramilli, A.S., D'Oliveira, A., Alford, T.L., Boffito, D.C. and Patience, G.S., 2020. Experimental methods in chemical engineering: X-ray diffraction spectroscopy—XRD. *The Canadian journal of chemical engineering*, 98(6), pp.1255-1266. <https://doi.org/10.1002/cjce.23747>
- [16] Hasan Taresh, B., Hadi Fakhri, F. and M Ahmed, L., 2022. Synthesis and characterization of CuO/CeO_2 nanocomposites and investigation their photocatalytic activity. *Journal of Nanostructures*, 12(3), pp.563-570. <https://doi.org/10.22052/JNS.2022.03.009>
- [17] Jaafar, M.T., Ahmed, L.M. and Haiwal, R.T., 2023. Solvent-Free Hydrothermal Synthesis of Network-Like Graphene Quantum Dots (GQD) Nano Particle and Ultrasonic TiO_2/GQD Nanocomposite. *Journal of Nanostructures*, 13(3), pp.626-638. <https://doi.org/10.22052/JNS.2023.03.003>
- [18] Obaid, A. and Ahmed, L., 2021. One-step hydrothermal synthesis of $\alpha\text{-MoO}_3$ nano-belts with ultrasonic assist for incorporating TiO_2 as a nanocomposite. *Egyptian Journal of Chemistry*, 64(10), pp.5725-5734. <https://doi.org/10.21608/ejchem.2021.72582.3615>

- [19] Ambroz, F., Macdonald, T.J., Martis, V. and Parkin, I.P., 2018. Evaluation of the BET Theory for the Characterization of Meso and Microporous MOFs. *Small methods*, 2(11), p.1800173. <https://doi.org/10.1002/smt.201800173>
- [20] DEBOER, J.H., 1953. The dynamical character of adsorption (Vol. 76, No. 2, p. 166). LWW. <https://journals.lww.com/soilsci/toc/1953/08000>
- [21] Donohue, M.D. and Aranovich, G.L., 1998. Classification of Gibbs adsorption isotherms. *Advances in colloid and interface science*, 76, pp.137-152. [https://doi.org/10.1016/S0001-8686\(98\)00044-X](https://doi.org/10.1016/S0001-8686(98)00044-X).
- [22] Thomas, S.P., Mansoor, H.H.A., Kullappan, M., Sethumathavan, V. and Natesan, B., 2019. Effect of Zeta Potential on Chitosan Doped Cerium Oxide in the Decolorization of Cationic Dye under Visible Light Irradiation. *Fibers and Polymers*, 20, pp.1418-1423. <https://doi.org/10.1007/s12221-019-8629-1>
- [23] Mohammad, H.M., Saeed, S.I. and Ahmed, L.M., 2023. Ease Synthesis of Broccoli-Like Fe₃O₄ Nanostructures for Superior Removal of Eosin Yellow Dye. *Journal of Nanostructures*, 13(2), pp.483-494. <https://doi.org/10.22052/JNS.2023.02.018>
- [24] Mohammad, H.M., Saeed, S.I. and Ahmed, L.M., 2022. Broccoli-like iron oxide nanoparticles synthesis in presence of surfactants and using them in the removal of water-colored contamination. *Journal of Nanostructures*, 12(4), pp.1034-1048. <https://doi.org/10.22052/JNS.2022.04.024>
- [25] Kadhem, F. H.; Ahmed, L.M., Abed S. A; Tami, A. N.; Wan Salleh, W. N., Friendly Green Synthesis of Cerium Oxide Nanoparticles Using *Citrus Aurantium* Extract and Applied in Removal of Eosin Yellow Dye, accepted in *Journal of Nanostructures*, 2025.
- [26] Binaeian, E., Zadvarzi, S.B. and Yuan, D., 2020. Anionic dye uptake via composite using chitosan-polyacrylamide hydrogel as matrix containing TiO₂ nanoparticles; comprehensive adsorption studies. *International journal of biological macromolecules*, 162, pp.150-162. <https://doi.org/10.1016/j.ijbiomac.2020.06.158>
- [27] Saeed, S.I., Attol, D.H., Eesa, M.T. and Ahmed, L.M., 2023, February. Zinc oxide-mediated removal and photocatalytic treatment of direct orange 39 dye as a textile dye. In *AIP Conference Proceedings* (Vol. 2414, No. 1). AIP Publishing. <https://doi.org/10.1063/5.0114787>

- [28] Temkin, M.J. and Pyzhev, V., 1940. Recent modifications to Langmuir isotherms. <https://sid.ir/paper/608793/en>
- [29] Khan, T.A. and Khan, E.A., 2015. Removal of basic dyes from aqueous solution by adsorption onto binary iron-manganese oxide coated kaolinite: non-linear isotherm and kinetics modeling. *Applied Clay Science*, 107, pp.70-77. <https://doi.org/10.1016/j.clay.2015.01.005>
- [30] Yatimzade, M.H., Ahmadpour, A., Ghahramaninezhad, M. and Sabzevar, A.M., 2024. Optimizing the efficient removal of ibuprofen from water environment by magnetic carbon aerogel: kinetics, isotherms, and thermodynamic studies. *Journal of Molecular Liquids*, 408, p.125337. <https://doi.org/10.1016/j.molliq.2024.125337>
- [31] Saeed, S.I., Taresh, B.H., Ahmed, L.M., Haboob, Z.F., Hassan, S.A. and Jassim, A.A.A., 2021. Insight into the Oxidant Agents Effect of Removal and Photodecolorization of Vitamin B 12 Solution in Drug Tablets using ZrO_2 . *Journal of Chemical Health Risks*, 11(4). DOI: 10.22034/jchr.2021.685757
- [32] Nandiyanto, A. B. D., Putri, M. E., Fiandini, M., Ragadhita, R., Kurniawan, T., Farobie, O., & Bilad, M. R. (2024). Characteristics of Ammonia Adsorption on Various Sizes of Calcium Carbonate Microparticles from Chicken Eggshell Waste, *Mor. J. Chem*, 12(3), 1073-1095. <https://doi.org/10.48317/IMIST.PRSM/morjchem-v12i3.48106>
- [33] Al-Fiydh, M.N., Najm, H.F., Karam, F.F. and Baqir, S.J., 2024. Thermodynamics, kinetic study and equilibrium isotherm analysis of cationic dye adsorption by ternary composite. *Results in Chemistry*, 10, p.101680. <https://doi.org/10.1016/j.rechem.2024.101680>
- [34] Mokhbi, Y., Ghiaba, Z., Akchiche, Z., Ghedamsi, R. and Reciou, B., 2024. Study of the adsorption mechanism of certain dyes from wastewater on commercial activated carbon using the Langmuir and Freundlich methods. *Studies in Engineering and Exact Sciences*, 5(2), pp.e5789-e5789. ojs.studiespublicacoes.com.br
- [35] Khit, S.A., Shaheed, I.M. and Kareem, E.T., 2023, July. A green synthesis of copper oxide nanoparticles using *Anchusa strigosa* L. flowers extract and study their impact for water pollutant removal. In *AIP Conference Proceedings* (Vol. 2830, No. 1). AIP Publishing. <https://doi.org/10.1063/5.0156952>

- [36] Santos, R., Silva, É.F., Dantas, E.J., Oliveira, E.D., Simões, T.B., Araújo, Í.R., Ribeiro, A.T., Oliveira, L.P., Garcia, R.R. and Almeida, L.C., 2020. Potential reuse of PET waste bottles as a green substrate/adsorbent for Reactive Black 5 dye removal. *Water, Air, & Soil Pollution*, 231, pp.1-16. <https://doi.org/10.1016/j.jclepro.2019.119448>
- [37] Langmuir, I., 1918. The adsorption of gases on plane surfaces of glass, mica and platinum. *Journal of the American Chemical society*, 40(9), pp.1361-1403. <https://doi.org/10.1021/ja02242a004>
- [38] Salih, S.J., Kareem, A.S.A. and Anwer, S.S., 2022. Adsorption of anionic dyes from textile wastewater utilizing raw corncob. *Heliyon*, 8(8). <https://doi.org/10.1016/j.heliyon.2022.e10092>
- [39] Temkin, M.J. and Pyzhev, V., 1940. Recent modifications to Langmuir isotherms. <https://sid.ir/paper/608793/en>
- [40] Georgi, A. and Kopinke, F.D., 2005. Interaction of adsorption and catalytic reactions in water decontamination processes: Part I. Oxidation of organic contaminants with hydrogen peroxide catalyzed by activated carbon. *Applied catalysis B: environmental*, 58(1-2), pp.9-18. <https://doi.org/10.1016/j.apcatb.2004.11.014>
- [41] Santos, V.P., Pereira, M.F., Faria, P.C.C. and Órfão, J.J., 2009. Decolourisation of dye solutions by oxidation with H₂O₂ in the presence of modified activated carbons. *Journal of hazardous materials*, 162(2-3), pp.736-742. <https://doi.org/10.1016/j.jhazmat.2008.05.090>
- [42] Fartode, A. P., & Parwate, D. V. (2014). Effect of H₂O₂ on UV Photolytic Remediation of Aqueous solutions of Methylene Blue. In *IOSR Journal of Applied Chemistry, International Conference on Advances in Engineering & Technology*, 69-72. www.iosrjournals.org
- [43] Alattar, R.A., Saleh, H.M., Al-Hilifi, J.A. and Ahmed, L.M., 2020. Influence the addition of Fe²⁺ and H₂O₂ on removal and decolorization of textile dye (dispersive yellow 42 dye). *Egyptian Journal of Chemistry*, 63(9), pp.3453-3463. <https://dx.doi.org/10.21608/ejchem.2020.23542.2400>
- [44] Bello, M.M., Raman, A.A.A. and Asghar, A., 2019. A review on approaches for addressing the limitations of Fenton oxidation for recalcitrant wastewater treatment. *Process Safety and Environmental Protection*, 126, pp.119-140. <https://doi.org/10.1016/j.psep.2019.03.028>

- [45] Borgohain, X., Das, E. and Rashid, M.H., 2023. Facile synthesis of CeO₂ nanoparticles for enhanced removal of malachite green dye from an aqueous environment. *Materials Advances*, 4(2), pp.683-693. <https://doi.org/10.1039/D2MA01019D>
- [46] Dadashi, R., Bahram, M., Farhadi, K., Asadzadeh, Z. and Hafezirad, J., 2024. Photodecoration of tungsten oxide nanoparticles onto eggshell as an ultra-fast adsorbent for removal of MB dye pollutant. *Scientific Reports*, 14(1), p.14478. <https://doi.org/10.1038/s41598-024-65573-5>